

Calculation of local excitations in large systems by embedding wave-function theory in density-functional theory

André Severo Pereira Gomes,^{*a} Christoph R. Jacob^{*ab} and Lucas Visscher^{*a}

Received 4th April 2008, Accepted 21st May 2008

First published as an Advance Article on the web 4th July 2008

DOI: 10.1039/b805739g

We present a simple and efficient embedding scheme for the wave-function based calculation of the energies of local excitations in large systems. By introducing an embedding potential obtained from density-functional theory (DFT) it is possible to describe the effect of an environment on local excitations of an embedded system in wave-function theory (WFT) calculations of the excitation energies. We outline the implementation of such a WFT-in-DFT embedding procedure employing the ADF, Dalton and DIRAC codes, where the embedded subsystem is treated with coupled cluster methods. We then evaluate this procedure in the calculation of the solvatochromic shift of acetone in water and of the *f*-*f* spectrum of NpO_2^{2+} embedded in a $\text{Cs}_2\text{UO}_2\text{Cl}_4$ crystal and find that our scheme does effectively incorporate the environment effect in both cases. A particularly interesting finding is that with our embedding scheme we can model the equatorial Cl^- ligands in $\text{NpO}_2\text{Cl}_4^{2-}$ quite accurately, compared to a fully wavefunction-based calculation, and this opens up the possibility of modeling the interaction of different ligands to actinyl species with relatively high accuracy but at a much reduced computational cost.

I. Introduction

Electronic excitations play an important role in several biological processes, such as photosynthesis and vision, as well as in technological applications like lighting materials. The information that computational chemistry is able to provide on such phenomena is helpful in the interpretation of complex experimental data (for reviews see, *e.g.*, ref. 1 and 2) and can be used in the development of new materials (see, *e.g.*, ref. 3).

To be of practical use, calculations should yield an accurate, preferably quantitatively correct, picture, but also be computationally efficient so that real-life systems can be tackled. Given its good balance between accuracy and computational efficiency, time-dependent density-functional theory (TDDFT)^{1,4,5} has become the standard *ab initio* approach for treating excited states of large-scale systems. Even though there are efforts towards having efficient wave-function based methods to calculate excitation energies,^{6–8} these remain computationally very expensive compared to TDDFT.

Full TDDFT calculations are, however, also limited to systems with up to a few hundred atoms, bringing calculations for still larger systems out of reach for routine application. This leaves the domain of large (biological) systems to subsystem methods that assume localization of the electronic excitations. The most employed approaches are hybrid quantum mechanics/molecular mechanics (QM/MM) methods,^{9–11}

that treat a central part in which the excitations of interest take place using a quantum mechanical method such as TDDFT, while its environment is described using molecular mechanics (for examples see, *e.g.*, ref. 12–16). However, in order to obtain accurate results, the force field used in the MM part has to be parametrized carefully, which is particularly difficult for heavy elements that display a variety of bonding interactions due to the many chemically accessible valence orbitals.

This weakness of the MM description can be overcome by considering a subsystem method with a QM description of the environment, the so-called QM/QM embedding schemes.^{17–20} Among these schemes, the ONIOM methods by Morokuma and co-workers^{17,18} are very popular. However, for the calculation of molecular properties these do not include the effect of the environment on the electronic structure of the embedded system, and are, therefore, only applicable as long as the property of interest can be adequately described by the lower-level method. Another example of such QM/QM schemes, that is particularly suited for studying localized excitations in solids is the *ab initio* model potential (AIMP) method.^{21–23} In this method, the effect of atoms or ions (or in a recent extension also larger fragments²⁴) in the environment of a subsystem of interest is included in the calculation of this active subsystem by means of nonlocal model potential obtained from Hartree–Fock theory. These model potentials contain, in addition to the electrostatic potential of the environment, projection operators to ensure the orthogonality between the wave functions of the active subsystem and the fragments in the environment.

A different QM/QM approach is taken in the frozen-density embedding (FDE) scheme by Wesolowski and Warshel,²⁵ in which both the system of interest and its environment are described using DFT (DFT-in-DFT). By basing the

^a Department of Theoretical Chemistry, Faculty of Sciences, Amsterdam Center for Multiscale Modeling, Vrije Universiteit Amsterdam, De Boelelaan 1083, 1081 HV Amsterdam, The Netherlands.

E-mail: gomes@few.vu.nl; visscher@chem.vu.nl

^b Present address: ETH Zurich, Laboratorium für Physikalische Chemie, Wolfgang-Pauli-Strasse 10, 8093 Zurich, Switzerland. E-mail: christoph.jacob@phys.chem.ethz.ch

formulation on DFT, it is possible to define a local embedding potential that only depends on the electron densities in the active subsystem and in the environment and does not contain any nonlocal projection operators. The FDE scheme has been shown to be both accurate and efficient for the calculation of solvent effects on electronic excitation energies^{26–28} as well as for the description of induced circular dichroism in guest–host complexes²⁹ and the electronic spectra of transition metal- and lanthanide-containing solids.^{30,31} Recently, it has been generalized to include the description of couplings between excitations in different subsystems,³² and it has been shown that this can be used to calculate excitation energy transfer couplings in natural light-harvesting systems.³³

Notwithstanding the success of the applications mentioned, the use of TDDFT in a pure DFT-in-DFT embedding scheme will encounter the limitations of TDDFT itself. Most important is the well-known problem in describing charge-transfer (CT) excitations,^{34–38} that are of particular importance in many biological systems and other systems exhibiting interesting photophysical properties.^{39–43} The DFT-in-DFT frozen density embedding scheme is able to remove spurious solvent–solute CT excitations but cannot solve the problem in cases where an intramolecular charge-transfer occurs. A second problem of a general nature is that, within the adiabatic approximation, TDDFT can only describe single excitations.^{44,45} Another problematic area for the application of TDDFT concerns excitations for heavy open-shell systems where inclusion of spin–orbit (SO) coupling is necessary already for a qualitative description of the system. Given the increasing interest in the organometallic and inorganic chemistry of molecules containing lanthanides, actinides and heavy transition elements,^{46,47} it is desirable to have alternative methods available that can handle such difficult cases.

An attractive way forward would be to combine the flexibility and accuracy of wave function theory (WFT) based methods with the efficiency of DFT. With subsystem methods one could then tackle the problems mentioned above, provided that the subsystem of interest can be chosen small enough to employ an accurate (relativistic) WFT approach. In this case, the FDE scheme offers a very distinct advantage over other schemes, since it employs the electron density, an observable quantity, and thereby avoids complicated problems like the definition of projection operators in calculations where the environment is to be treated by one-component DFT while the active system is described by a 4-component relativistic WFT method. Such a WFT-in-DFT embedding scheme based on the DFT-in-DFT frozen-density embedding scheme has first been proposed by Carter and coworkers,^{48–50} where DFT and variational methods such as Hartree–Fock, CASSCF or (multireference)-CI were combined. This approach was mainly used to describe localized properties in solids or surfaces, *e.g.* for the calculation of excitation energies of CO adsorbed on a platinum surface.^{51,52}

In this paper, we aim to introduce a simplified and computationally less involved version of this WFT-in-DFT embedding scheme for the calculation of local excitations in large systems. In particular, we apply coupled cluster methods for the treatment of an embedded system and describe the environment by DFT. We test this approach for two different

systems. First, as a benchmark application, we revisit the calculation of the solvatochromic shift of acetone in water that was previously performed by Neugebauer *et al.*²⁶ Second, as an example for a system where the WFT-in-DFT treatment of the excitations is essential, we investigate the *f–f* spectrum of neptunyl (NpO₂²⁺) embedded in the Cs₂UO₂Cl₄ crystal, following our previous study of the isolated neptunyl ion with relativistic coupled cluster methods.⁵³

The outline of the paper is as follows. In section II we present the essential theoretical aspects of WFT-in-DFT embedding methods and outline the proposed scheme. In section III, we then describe our implementation, as well as other computational details. This is followed by the two sample applications of the proposed scheme. In section IVA, the results obtained for acetone solvated in water are presented, and in section IVB, the spectrum of neptunyl embedded in a Cs₂UO₂Cl₄ crystal is discussed. Finally, concluding remarks are given in section V.

II. Theory

In the formulation of the WFT-in-DFT frozen density embedding scheme proposed by Carter and coworkers,^{48–51} the total system is partitioned into an embedded subsystem I and its environment, so that the total energy for the system can be expressed as

$$E[\Psi_I^{\text{WFT}}, \rho_{\text{II}}^{\text{DFT}}] = E_I[\Psi_I^{\text{WFT}}] + E_{\text{II}}[\rho_{\text{II}}^{\text{DFT}}] + E_{\text{int}}[\rho_I^{\text{WFT}}, \rho_{\text{II}}^{\text{DFT}}], \quad (2.1)$$

where E_I is the energy of the embedded subsystem I, described using a wavefunction-based method and characterized by its wave function Ψ_I^{WFT} , while E_{II} is the energy of the environment (subsystem II), described using DFT and characterized by its electron density $\rho_{\text{II}}^{\text{DFT}}$. The interaction energy E_{int} is defined within DFT as

$$E_{\text{int}}[\rho_I, \rho_{\text{II}}] = E_{\text{NN}} + \int \rho_I(\mathbf{r})v_{\text{II}}^{\text{nuc}}(\mathbf{r})d\mathbf{r} + \int \rho_{\text{II}}(\mathbf{r})v_I^{\text{nuc}}(\mathbf{r})d\mathbf{r} + \frac{1}{2} \int \frac{\rho_I(\mathbf{r})\rho_{\text{II}}(\mathbf{r}')}{|\mathbf{r}-\mathbf{r}'|}d\mathbf{r}d\mathbf{r}' + E_{\text{xc}}^{\text{nadd}}[\rho_I, \rho_{\text{II}}] + T_s^{\text{nadd}}[\rho_I, \rho_{\text{II}}] \quad (2.2)$$

where the density of subsystem I ($\rho_I \equiv \rho_I^{\text{WFT}}$) is the density obtained from the wave function treatment, while the environment density ($\rho_{\text{II}} \equiv \rho_{\text{II}}^{\text{DFT}}$) is to be obtained from a DFT calculation. In this expression for the interaction energy, E_{NN} is the nuclear–nuclear repulsion energy, v_I^{nuc} and $v_{\text{II}}^{\text{nuc}}$ are the electrostatic potentials of the nuclei in subsystems I and II, respectively, $E_{\text{xc}}^{\text{nadd}}[\rho_I, \rho_{\text{II}}] = E_{\text{xc}}[\rho_I + \rho_{\text{II}}] - E_{\text{xc}}[\rho_I] - E_{\text{xc}}[\rho_{\text{II}}]$ is the nonadditive part of the exchange–correlation energy, and $T_s^{\text{nadd}}[\rho_I, \rho_{\text{II}}] = T_s[\rho_I + \rho_{\text{II}}] - T_s[\rho_I] - T_s[\rho_{\text{II}}]$ is the nonadditive kinetic energy, where T_s is the kinetic energy of the Kohn–Sham noninteracting reference system.

To include the effect of the environment in the WFT calculation of subsystem I, Carter and coworkers proposed⁴⁸ to include an embedding potential given, in analogy to the DFT-in-DFT frozen-density embedding scheme of

Wesolowski and Warshel,²⁵ by the functional derivative of $E_{\text{int}}^{\text{DFT}}$ with respect to ρ_I ,

$$v_{\text{eff}}^{\text{emb}}[\rho_I, \rho_{\text{II}}](\mathbf{r}) = v_{\text{II}}^{\text{nuc}}(\mathbf{r}) + \int \frac{\rho_{\text{II}}(\mathbf{r}')}{|\mathbf{r} - \mathbf{r}'|} d\mathbf{r}' + \frac{\delta E_{\text{xc}}^{\text{nadd}}[\rho_I, \rho_{\text{II}}]}{\delta \rho_I} + \frac{\delta T_s^{\text{nadd}}[\rho_I, \rho_{\text{II}}]}{\delta \rho_I}. \quad (2.3)$$

This embedding potential includes the electrostatic potentials of the nuclei and the electron density in the environment, as well as contributions arising from the nonadditive part of the exchange–correlation energy and from the nonadditive kinetic energy. Since this embedding potential depends on the density of subsystem I it has to be updated iteratively during the WFT calculation.

While the theoretical justification of the use of such an embedding potential derived from DFT in wave function based calculations was previously debated,^{54,55} Wesolowski recently showed⁵⁶ that for exact density functionals and a full CI expansion of the wave function, the above approach will indeed lead to the exact total electron density $\rho_I + \rho_{\text{II}}$. If a truncated expansion of the wave function is employed, an additional term that corrects for the deficiency of the WFT description, could be included in the embedding potential to keep the theory formally exact. Since such a term will be the less important the closer the WFT description is to full CI and, moreover, since it is neither possible nor desirable to correct the error introduced by a poor WFT description by means of DFT, we consider it well justified to neglect this term and simply employ the uncorrected embedding potential given above.

In the practical application of the WFT-in-DFT embedding scheme described above, several additional approximations will be introduced. First, neither the DFT treatment nor the WFT treatment can be exact. In the DFT case, this is due to the well-known deficiencies in the currently available exchange–correlation functionals, in the WFT case due to the infeasibility to employ a full CI expansion in a large basis for anything but the smallest model systems. Second, the nonadditive kinetic energy component of the embedding potential is evaluated using an approximate kinetic energy functional. Several applications of the DFT-in-DFT frozen-density embedding scheme show that the available kinetic energy functionals provide a reliable description, in the case of weakly bonded complexes^{57–59} and solute–solvent interactions^{26–28,60,61} or in simple solid-state systems.^{30,31,62–66} For strongly bound covalent systems one needs to resort to other solutions, *e.g.*, employ a 3-partitioning scheme introducing capping groups with a constrained electron density that has recently been developed by two of us.⁶⁷

For efficiency reasons it is furthermore common to employ approximations in the construction of the electron density of the environment ρ_{II} . In the simplest case, the electron density is obtained as a sum of fragment densities that is kept completely frozen in the following calculations. This choice is still in principle exact as long as the density of the environment is everywhere smaller than the exact total density of the full system. In case of strong polarization, the simple sum-of-fragments approximation for the environment density may

easily violate the latter condition. In such cases it is necessary to consider the relaxation of the environment under the influence of the embedded subsystem. As for DFT-in-DFT embedding, this is possible by employing so-called freeze-and-thaw cycles,⁶⁸ *i.e.*, by interchanging the roles of the two subsystems and updating the density of the environment in a DFT calculation that includes the effect of subsystem I *via* the embedding potential $v_{\text{eff}}^{\text{emb}}[\rho_{\text{II}}, \rho_I]$. This can be repeated iteratively until convergence is reached.

For the application of WFT-in-DFT embedding to atoms and molecules adsorbed on surfaces, Carter and coworkers proposed different simplified schemes for performing the freeze-and-thaw cycles and obtaining a self-consistent embedding potential. In their initial work,^{49,51,52} the total density $\rho_{\text{tot}} = \rho_I + \rho_{\text{II}}$ was obtained from a DFT calculation with periodic boundary conditions. This total density was then kept fixed, while ρ_I and ρ_{II} were updated subsequently, based on the density ρ_I^{WFT} of the WFT calculation of the adsorbed molecule. In later work,⁵⁰ they modified this scheme such that the density $\rho_{\text{II}} = \rho_{\text{tot}} - \rho_I^{\text{bare}}$ is kept frozen, where ρ_{tot} is again obtained from a DFT calculation, while ρ_I^{bare} is taken from a WFT calculation on the isolated subsystem I.

However, for the calculation of excitation energies using WFT-in-DFT embedding, it may be that a simpler approach can be employed. In many cases where TDDFT is known to fail, such as for charge-transfer excitations or for open-shell systems with close-lying excited states, it is still possible to obtain an accurate description of the ground-state density from a DFT treatment. When the ground state is well described by DFT, it should be possible to first calculate an approximation of both ρ_I and ρ_{II} using DFT-in-DFT embedding (possibly employing freeze-and-thaw cycles) and to subsequently use the embedding potential constructed using these densities in the WFT calculation of the excitation energies of the embedded system. This is quite different from the cases studied by Carter and coworkers, who investigated excitation energies of molecules adsorbed on surfaces,^{51,52} where already the description of the ground-state in DFT is problematic.⁴⁹

This means that in eqn (2.3), instead of the density ρ_I^{WFT} obtained from the WFT calculation, the DFT density for subsystem I, ρ_I^{DFT} , obtained from a DFT-in-DFT embedding calculation, is used. If such a simplified treatment is justified, it offers several advantages over the self-consistent WFT-in-DFT schemes described above. First, only one computationally expensive WFT calculation is required, compared to the multiple calculations required to converge a freeze-and-thaw procedure. Second, it is not necessary to generate the density ρ_I^{WFT} , thereby avoiding a non-trivial and computationally expensive step in non-variational WFT approaches that employ intermediate normalization. Finally, also the embedding potential has to be calculated only once, instead of updating it during the iterative solution of the Hartree–Fock and CC equations. This latter simplification is similar to the linearization of the embedding potential recently proposed in DFT-in-DFT frozen-density embedding.⁶⁹

The calculation of excitation energies in particular (or of response properties in general) can be carried out with a generalization of the theory outlined above. We again make the assumption that the WFT method will be able to yield a

close enough approximation to the exact density response of the subsystems. While in the case of static embedding theory this is in principle true for a full CI calculation in a saturated basis, we now have the additional limitation that we can only account for the response of the active system.

This limitation is usually also present in implementations of DFT-in-DFT, although Neugebauer³² has recently presented a sophistication of the theory by Casida and Wesolowski⁷⁰ that makes it possible to treat also the case of coupled excitations in extended systems. For our initial application we consider the latter scheme and even make a further approximation in neglecting any variations on the embedding potential due to the response of the active subsystem to the external perturbations, which for TDDFT excitation energies are incorporated by including the derivative of the embedding potential in the kernel.⁷⁰ This means that in effect we always consider a fixed embedding potential based on the ground-state density.

This additional approximation is valid as long as the non-additive kinetic and exchange–correlation potentials of the initial and final states are not too different, which will be the case if the excitation is truly localized in the interior of the embedded subsystem, as is known to be the case in the applications considered in this work.

III. Implementation and computational details

In our implementation, we use a combination of different quantum chemical program packages. In the first step, ADF^{71,72} and the implementation of the DFT-in-DFT frozen-density embedding scheme in this package^{27,73} are employed for obtaining an approximation to the density of subsystem I, ρ_I^{DFT} , and to calculate the embedding potential $v_{\text{eff}}^{\text{emb}}[\rho_I^{\text{DFT}}, \rho_{\text{II}}]$. The values of this embedding potential on the points of the integration grid generated by ADF are stored in a file for later use in the WFT calculation.

In the present work, we will always start by approximating the density of the environment as a sum of the densities of molecular or atomic fragments that were calculated for the isolated fragments. As fragments we either used the distinct water molecules in the solvent environment of acetone in water, or the $\text{UO}_2\text{Cl}_4^{2-}$, Cs^+ , and Cl^- units that constitute the $\text{Cs}_2\text{UO}_2\text{Cl}_4$ crystal environment. Details on the construction of the environment density will be given below. In the case of acetone solvated in water, the simplest approximation of the solvent environment as a sum of fragments was previously shown to be a sufficiently accurate description.²⁶ For the crystal environment, a detailed study of the different possibilities for constructing the environment density is outside the scope of this work, and will be addressed in another publication that deals with excitations in the pure $\text{Cs}_2\text{UO}_2\text{Cl}_4$ crystal.⁷⁴ We first consider the sum of fragments approach described above and improve on this simple approximation, by employing the freeze-and-thaw procedure only for the nearest-neighbor Cl^- ions.

In the calculation of the fragments used for the construction of the frozen density, we used for the solvent water environment the local-density approximation (LDA)⁷⁵ for the exchange–correlation potential and a DZP basis set from the

ADF basis set library.^{71,76} For the fragments used to model the $\text{Cs}_2\text{UO}_2\text{Cl}_4$ crystal environment, we used the statistical averaging of model orbital potentials (SAOP),⁷⁷ in combination with a TZ2P basis set. In this case, scalar relativistic effects were included *via* the zeroth-order regular approximation (ZORA).⁷⁸ In all cases, we employed a spin-restricted closed-shell description of the frozen environment density.

To model the density of the active system in the DFT-in-DFT frozen-density embedding calculations for acetone and neptunyl we employed the SAOP functional and the TZ2P basis set. The nonadditive kinetic-energy component of the embedding potential was modeled by the PW91k functional,⁷⁹ while the exchange–correlation component was treated using the Becke–Perdew–Wang (BPW91) exchange–correlation functional.^{80,81} For the neptunyl calculations, spin-unrestricted DFT calculations were performed, and scalar relativistic effects were included *via* the zeroth-order regular approximation (ZORA).⁷⁸

After generating the embedding potential, we used a locally modified version of DALTON⁸² for nonrelativistic WFT calculations and a development version of DIRAC⁸³ for relativistic WFT calculations. In the nonrelativistic case, matrix elements of $v_{\text{eff}}^{\text{emb}}(r)$ are constructed as

$$v_{ij} = \langle \phi_i | v_{\text{eff}}^{\text{emb}} | \phi_j \rangle \approx \sum_k w_k v_{\text{eff}}^{\text{emb}}(\mathbf{r}_k) \phi_i(\mathbf{r}_k) \phi_j(\mathbf{r}_k), \quad (3.4)$$

where $\phi_i(\mathbf{r}_k)$ is the value of orbital ϕ_i evaluated at grid point \mathbf{r}_k and w_k is the integration weight associated with this grid point. It should be noted that we employ the accurate numerical integration grid used by ADF, which is also able to integrate the electrostatic terms appearing in the embedding potential accurately.^{27,84} In a relativistic framework the embedding potential, being a scalar potential, enters the one-electron Hamiltonian as a diagonal operator expressed (in 2-component form) as

$$v_{\text{eff}}^{\text{emb}}(\mathbf{r}) = \begin{pmatrix} v_{\text{eff}}^{\text{emb}}(\mathbf{r}) & \mathbf{0} \\ \mathbf{0} & v_{\text{eff}}^{\text{emb}}(\mathbf{r}) \end{pmatrix}. \quad (3.5)$$

Therefore, the matrix elements of the embedding potential with respect to spinors $\phi_i(r)$ and $\phi_j(r)$ are given by

$$v_{ij} = \langle \phi_i | v_{\text{eff}}^{\text{emb}} | \phi_j \rangle \approx \sum_k w_k v_{\text{eff}}^{\text{emb}}(\mathbf{r}_k) [\phi_i^L(\mathbf{r}_k) \phi_j^L(\mathbf{r}_k) + \phi_i^S(\mathbf{r}_k) \phi_j^S(\mathbf{r}_k)] \quad (3.6)$$

where $\phi_{i,j}^L(\mathbf{k})$ and $\phi_{i,j}^S(\mathbf{k})$ are scalar functions for the large and small components, respectively. Once the embedding potential matrix is set up, it is added to the one-electron Fock matrix in the WFT calculation, like any other one-electron operator.

For the calculation of the excitation energies of acetone solvated in water, we employed the CC2 method^{85–87} as implemented in DALTON.⁸² The aug-cc-pVDZ basis set was used for acetone,⁸⁸ as it has previously been shown⁸⁹ that CCSD excitation energies are essentially converged with this basis sets, and the same behavior is expected for CC2. In the CC2 calculations the 1s orbitals of all atoms are kept frozen.

The calculations of the excitation spectrum of neptunyl were performed with DIRAC⁸³ using the exact two-component (X2C) approach recently outlined by Iliaš and Saue,⁹⁰ with spin–orbit coupling being included in the latter *via* mean-field

integrals, calculated with the AMFI code.^{91,92} A valence double zeta basis by Dyll⁹³ was used for Np whereas the aug-cc-pVTZ basis⁸⁸ was used for O (and for Cl where applicable). In the correlated calculations the intermediate Hamiltonian Fock-space coupled-cluster (IHfSCC) method^{94–96} was used. In the IHfSCC calculations we start from a closed shell (NpO_2^{3+} or $\text{NpO}_2\text{Cl}_4^-$) species and obtain the excitation spectrum of the target system (NpO_2^{2+} or $\text{NpO}_2\text{Cl}_4^{2-}$) from the $(0h,1p)$ sector. We have used a slightly smaller active space than employed previously for NpO_2^{2+} ,⁵³ consisting of about the same number of virtual spinors (75 and 76, respectively) for both species in the correlated calculations. Of these, 6 are kept in the P_m space and 19 in the P_I space. The number of occupied spinors included for NpO_2^{2+} and $\text{NpO}_2\text{Cl}_4^{2-}$ are 12 and 28, respectively. We note that due to the presence of the frozen environment, the symmetry in the wavefunction calculations is reduced to C_1 , and the IHfSCC calculations are, therefore, significantly more expensive than the original NpO_2^{2+} calculations that could exploit the $D_{\infty h}$ symmetry.

In order to automate both the initial DFT-in-DFT calculations and the interoperation of the different quantum chemical packages, we made use of the recently developed PYADF scripting framework.⁹⁷

IV. Results and discussion

A Solvatochromic shifts of acetone in water

The determination of solvatochromic shifts of acetone in water is an ideal benchmark for our method because it has been extensively studied with a range of WFT methodologies, taking into account solvent effects in different ways (see ref. 89 and references therein). Furthermore, Neugebauer *et al.* have previously performed a systematic study²⁶ on this system using DFT-in-DFT frozen-density embedding.

We have employed the set of geometries obtained in ref. 26 from Car–Parrinello molecular dynamics (CP-MD) simulations of both the gas-phase and the solution. From these simulations, 300 and 220 snapshots were retained for the calculations in the gas-phase and in solution, respectively (Fig. 1). The excitation energies of the $n \rightarrow \pi$ transition are then calculated as a weighted average over these snapshots, using the oscillator strengths as weight factors.

We note that our reference DFT-in-DFT calculations differ slightly from the values obtained by Neugebauer and co-workers as we could apply a larger basis set than was feasible with the previous implementation of DFT-in-DFT that was used in ref. 26. Irrespective of these small differences, one of the findings of Neugebauer *et al.* that is very relevant for this work has to do with the construction of the density for the frozen subsystem: they observed nearly identical solvent shifts (differences of about 0.01 eV or less) when the embedding potential was constructed from an approximate density, made up by the superposition of densities obtained for isolated water molecules, compared to when densities from calculations including all waters at once were used to obtain the embedding potential. For this system, different functionals used to produce the density of these unperturbed solvent molecules

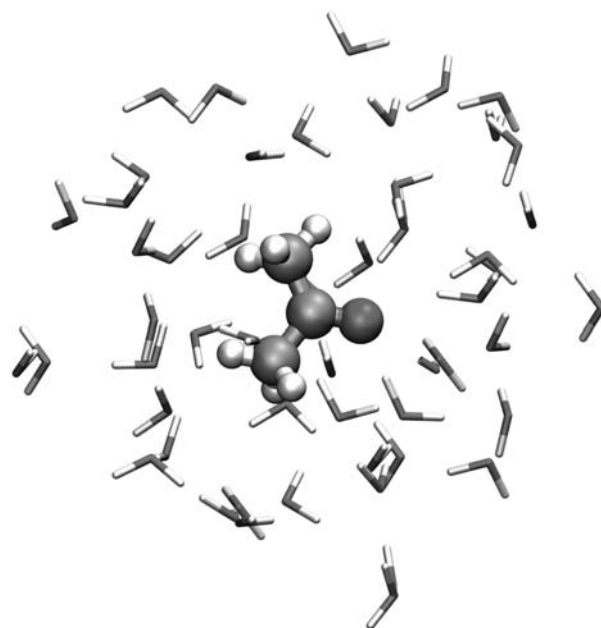


Fig. 1 CP-MD snapshot for the simulation of acetone in water.

were proven to yield similar results, which is why we chose the simple LDA functional for this purpose.

The calculated excitation energies are summarized in Table 1. Inspecting first the CC2 results, one observes a very good agreement with experiment for the solvent shift. This indicates that the embedding potential generated in the underlying DFT-in-DFT calculations does indeed provide a realistic representation for the solute–solvent interaction. Moreover, it also indirectly validates our initial assumptions, that is, that the ground state density of the active subsystem calculated with DFT is nearly identical to the corresponding wavefunction-based density and that the direct contribution of the environment to the response is negligible. To verify the latter assumption we also carried out additional DFT-in-DFT calculations in which the embedding contributions to the kernel were switched off.²⁸ These calculations indicate that this contribution amounts to 1 meV for the lowest $n \rightarrow \pi$ excitation energy that we consider in this work. Other excitations show somewhat larger shifts, but these are generally at least one order of magnitude smaller than the corresponding solvatochromic shift. The state for which the neglect of the response contribution has the largest effect (about 0.03 eV) is the fifth singlet excited state, located at about 8 eV.

The quality of the TDDFT results with the DZP/TZ2P combination appears to be not as good as for the CC2 calculations with as most significant difference an underestimation of the solvent shift. Furthermore, one sees significant basis set effects on the TDDFT results if a crude description for the solvent (DZ) is used, as done previously,²⁶ with a fortuitous cancellation of errors in the shift for the DZ calculation. One should thereby note, however, that for CC2 both the gas-phase and solution excitation energies are underestimated in comparison to the corresponding experimental values, putting the TDDFT results closer to experiment. Since roughly identical discrepancies are found for results in the

Table 1 TD-DFT and CC2 $n \rightarrow \pi$ excitation energies ($\langle \omega_i \rangle$, in eV) for acetone in gas-phase and solution, calculated as oscillator strength-weighted averages over the CP-MD snapshots, together with the corresponding solvatochromic shifts. For comparison, the CCSD results of Aidas and coworkers⁸⁹ as well as experimental results are also shown

Method	Basis sets		$\langle \omega_i \rangle$		
	Acetone	Water	Gas phase	Solution	Shift
TD-DFT	TZP	DZ	4.464	4.667	0.203
	TZ2P	DZP	4.471	4.636	0.165
CC2	TZ2P/aug-cc-pVDZ		4.350	4.546	0.196
CCSD (ref. 89)			4.491	4.686	0.195
Exp. (ref. 106–108)			4.48–4.49	4.68–4.69	0.19–0.21

gas-phase and solution, this cannot be attributed to inaccuracies in the embedding procedure.

A possible explanation for the underestimated CC2 excitation energies is the sensitivity to the chosen structures of the acetone molecule. The results of Aidas and coworkers⁸⁹ show a significant dependence of the excitation energies on the C=O bond distance, where larger distances lower the excitation energies. To test this, we performed a series of test calculations at the equilibrium structures that were obtained using DFT-BLYP (the functional that was used in the CP-MD simulations), DFT-B3LYP, and CCSD. The equilibrium structures and corresponding CC2 excitation energies are summarized in Table 2. The results show that DFT-BLYP overestimates the C=O bond distance, which leads to an underestimation of the CC2 excitation energy. Since the CP-MD structures that we used were based on a simulation performed with the BLYP functional this explains part of the error in the comparison to the experimental data. Since the error is due to a bond length that is found consistently too long in both the gas-phase and in solution structures, only the absolute values but not the solvatochromic shift are affected.

B f - f spectrum of $\text{Cs}_2\text{U}(\text{Np})\text{O}_2\text{Cl}_4$

As a second, more challenging application, we apply WFT-in-DFT embedding to the calculation of the f - f spectrum of the neptunyl cation (NpO_2^{2+}). The spectrum of the isolated neptunyl cation was investigated previously in our group.⁵³ The available experimental neptunyl spectra were taken from impurities in host crystals such as $\text{Cs}_2\text{UO}_2\text{Cl}_4$ or $\text{CsUO}_2(\text{NO}_3)_3$.^{98,99} To be able to compare directly to these data one thus needs to model the host crystal as well. There has been one such attempt before by Matsika and Pitzer,¹⁰⁰ who performed a calculation on $\text{Cs}_2\text{U}(\text{Np})\text{O}_2\text{Cl}_4$ using a cluster model. In their treatment, a central $\text{NpO}_2\text{Cl}_4^{2-}$ unit is treated using SO-CI, with the six nearest-neighbor caesium atoms described by all-electron model potentials and all other species up to 25 Å away from the central actinyl unit as point charges.

Table 2 CC2 $n \rightarrow \pi$ excitation energies ($\omega_{n \rightarrow \pi}$, in eV) for acetone in the gas-phase at equilibrium geometries obtained with different methods. All calculations have been performed using the aug-cc-pVDZ basis set

Geometry	$r_{\text{CO}}/\text{Å}$	$\omega_{n \rightarrow \pi}/\text{eV}$
BLYP	1.2302	4.442
B3LYP	1.2175	4.535
CCSD	1.2217	4.505

To include the effect of the crystal environment in our relativistic IHFSCC calculations,⁵³ we employ a similar partitioning as used in recent applications of DFT-in-DFT frozen-density embedding for transition metal- and lanthanide-containing solids.^{30,31} In our case we devise a cluster model, where the active subsystem is treated with relativistic IHFSCC theory and DFT is used to model the nearby ions that may overlap with the impurity (Fig. 2). The Madelung potential arising from the rest of the crystal was evaluated using formal charges placed at the positions given by the X-ray structure of the pure crystal.¹⁰¹ We thereby utilized¹⁰² the program ENV^{103,104} to determine the extent of the intermediate region encapsulating the central active subsystem as well as an array of surrounding point charges that describe the Madelung potential for the crystal. This intermediate region always comprises 20 $\text{UO}_2\text{Cl}_4^{2-}$ and 90 Cs^+ ions. In the central unit we have replaced the uranium by neptunium, and adjusted the Np–O and Np–Cl bond lengths to those from the X-ray structure for $\text{NpO}_2\text{Cl}_4^{2-}$.¹⁰⁵ We explored two different possibilities for the central unit: (a) one where it was split into NpO_2^{2+} and Cl_4^{4-} , and only NpO_2^{2+} was treated using IHFSCC, while the ligands were taken into account with different degrees of sophistication (from simple point charges to densities fully relaxed in freeze-and-thaw cycles); and (b) one where the entire $\text{NpO}_2\text{Cl}_4^{2-}$ is calculated with IHFSCC.

Our results are summarized in Table 3, which displays the symmetry classification and excitation energies for the different f - f states following the ordering found in the experimental

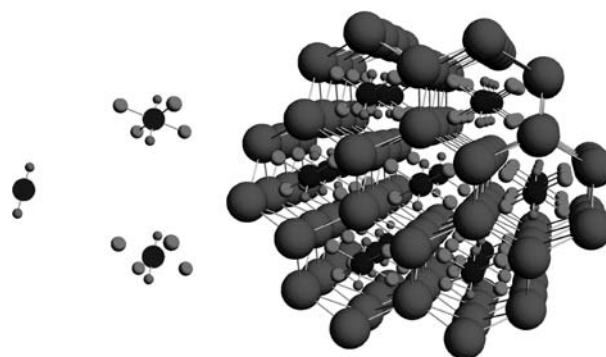


Fig. 2 Steps in the WFT-in-DFT embedding calculation on the f - f spectrum of $\text{Cs}_2\text{U}(\text{Np})\text{O}_2\text{Cl}_4$. From left to right, (a) the initial NpO_2^{2+} ion (b) is surrounded by four chlorides (top: chlorides considered explicitly in the WFT calculations; bottom: ligand group Cl_4^{4-} is taken as part of the environment and included *via* the embedding potential) to make up the central unit in the cluster model; and (c) this unit is embedded into a larger environment. The larger model is then embedded in an array of point charges (not shown).

Table 3 f - f excited state energies (in cm^{-1}) for NpO_2^{2+} and $\text{NpO}_2\text{Cl}_4^{2-}$, obtained with and without the inclusion of environment effects via WFT-in-DFT embedding. All calculations were performed using the X-ray structure reported in ref. 101 (where $r_{\text{NpO}} = 1.775$ and $r_{\text{NpCl}} = 2.653$ Å, respectively) unless otherwise noted. For comparison, the results of Matsika and Pitzer¹⁰⁰ for their embedded cluster calculations are shown, together with the experimental values due to Denning and coworkers⁹⁸

Central unit	Surrounding	Excited electronic states				
		I	II	III	IV	V
NpO_2^{2+}	—	$\Delta_{3/2u}$	$\Delta_{5/2u}$	$\Phi_{7/2u}$	$\Pi_{1/2u}$	$\Pi_{3/2u}$
IHFSCC ^a	—	3221	8565	7225	30 877	34 947
IHFSCC	—	4297	9661	7229	29 021	32 379
$\text{NpO}_2^{2+} \text{L}_4^{-4}$	—	$\Delta_{3/2u} + \Phi_{5/2u}$	$\Delta_{5/2u}$	$\Phi_{7/2u}$	$\Pi_{1/2u}$	$\Pi_{3/2u}$
IHFSCC point charges	—	2093	8032	7828	23 326	26 321
IHFSCC DFT (frozen) ^b	—	2243	8150	7677	23 323	26 433
IHFSCC DFT (relaxed) ^c	—	1034	7307	8029	20 390	23 303
$\text{NpO}_2\text{Cl}_4^{2-}$	—	$\Delta_{3/2u} + \Phi_{5/2u}$	$\Delta_{5/2u}$	$\Phi_{7/2u}$	$\Pi_{1/2u}$	$\Pi_{3/2u}$
IHFSCC	—	886	7679	9262	20 018	22 445
IHFSCC	DFT ^d	1156	7738	9137	20 857	26 305
$\text{NpO}_2\text{Cl}_4^{2-}$ (ref. 100)	—	$\Phi + \Delta$	$\Delta + \Phi$	Φ	Π	Π
SO-Cl	AIMP ^e	1663	5775	8463	18 367	20 575
Exp. (ref. 98)	—	$\Delta_{3/2u} + \Phi_{5/2u}$	$\Delta_{5/2u}$	$\Phi_{7/2u}$	$\Pi_{1/2u}$	$\Pi_{3/2u}$
		900–1050	6880	7890	17 241	20 081

^a Using the gas-phase geometry with $r_{\text{NpO}} = 1.675$ Å (from the calculations of ref. 53). ^b Frozen density for the ligand group (L_4^{-4}) constructed as superposition of the densities of four Cl^- ions. ^c Frozen density for the ligand group (L_4^{-4}) obtained for Cl_4^{-4} after 10 freeze-and-thaw cycles. ^d $[\text{Cs}_{90}(\text{UO}_2\text{Cl}_4)_{20}]^{+50}$ in the presence of point charges that counterbalance its and the active subsystem's charge. ^e Model potential obtained for the six-nearest caesium atoms plus a point charge array.

assignment of these transitions. Considering first the case where only the bare NpO_2^{2+} (with the Np–O bond length from the X-ray geometry¹⁰⁵) unit is chosen as central unit, we see that these gas-phase results tend to strongly overestimate the excitation energies in comparison to experiment (about 3000 cm^{-1} for states **I** and **II** and about $12\,000 \text{ cm}^{-1}$ for states **IV** and **V**) with the exception of state **III**, for which gas-phase results underestimate the excitation energy by only 650 cm^{-1} . Compared to the energies at the optimized equilibrium geometry for the gas-phase (where $r_{\text{Np-O}} = 1.675$ Å), the values at the X-ray geometry are about 1000 cm^{-1} higher for **I** and **II**, and lower for **IV** and **V** by roughly the same amount. The excitation energy for state **III** is, however, almost not affected by the change in distance. This is easily explained by the fact that this is the pure $\Phi_{7/2u}$ state, that is fully localized on the Np atom and forms the higher spin–orbit component of the $\Phi_{5/2u}$ ground state. The other states have some covalent character that makes them more susceptible to changes in the distance to the oxo-groups.

Before considering the full cluster model, we first consider the equatorial ligands that will have the strongest effect on the excitation energies. The ligand field breaks the linear symmetry of the actinyl and induces mixing between the lowest spin–orbit components of the Δ and Φ states, while charge-transfer from the formally negative chloride ions to the neptunium center of the dication weakens the axial bonds of the neptunyl. In order to assess the relative importance of these effects, we present in Table 3 calculations with varying degrees of sophistication in the treatment of this ligand group.

In the simplest case the NpO_2^{2+} species is surrounded by four point charges at the position of the chlorides, each with a negative unit charge. This has a very strong effect on four of the levels, with downward shifts of 2204 cm^{-1} for state **I**, 1629 cm^{-1} for **II**, 5695 cm^{-1} for **IV** and 8626 cm^{-1} for **V**, respectively.

State **III** is shifted upwards by 599 cm^{-1} by the presence of the point charges. From the composition of these states in the FSCC wave function, we see that there is a considerable mixing between the $\Delta_{3/2u}$ and $\Phi_{5/2u}$ states in the ground and first excited states, while the others remain pure states. Compared to the experimental results, all excitation energies are improved significantly by this simple electrostatic model. We see that apart from **III** the calculated excitation energies are too high by about 1000 cm^{-1} for **I** and **II** and about 5000 cm^{-1} for **IV** and **V**. State **III** is very close to the experimental value, being only 62 cm^{-1} lower.

More sophisticated models for the ligands where these are represented by an embedding potential, are considered next. The first approach is to have a frozen density constructed as a superposition of atomic densities for the chloride ions. From our results it can be seen that this simplest FDE model hardly changes the point charge picture—in fact, there is even a slightly worse agreement with experiment for all states but **IV**, by about 100 – 150 cm^{-1} . The problem comes from the fact that the charge density for the Cl^- ligands is by construction spherical so that the significant deformation and charge transfer towards the actinyl ion should be accounted for in the calculation of the active system. This is not possible as one can in FDE describe only the flow of charge towards the frozen system and not that from the frozen system. To remedy this problem we have performed 10 freeze-and-thaw cycles to allow for such relaxation. After this procedure a completely different picture emerges. Excitation energies for states with Δ and/or Φ character agree within 100 – 450 cm^{-1} with the experimental data, whereas the error for the **II** states is reduced to about 3200 cm^{-1} . This leads to a much better overall agreement with experiment, with now a correct ordering of the states **II** and **III**. The only exception is the **III** state that is moved to somewhat higher energies by the relaxation of the density.

To make a precise assessment of the quality of the embedding it is, however, better to not compare it directly to the experimental data but compare the subsystem treatment of the ligands in the IHFSCC calculation to a supermolecular calculation of $\text{NpO}_2\text{Cl}_4^{2-}$. This case can be seen as an exact reference for the above embedding calculations, since in both cases no outer environment was included. Moving from the embedding calculation where the Cl^- densities are relaxed, to a supermolecular calculation has the overall result of a slight increase of the excitation energies of all states: state **I** is shifted by about 150 cm^{-1} , while shifts of about 370 cm^{-1} are seen for **II** and **IV**. For **III** and **V** the shifts lie in the $860\text{--}1200\text{ cm}^{-1}$ range. This indicates that in this case, where the actinide–chloride bond is known to have significant ionic character, the WFT-in-DFT embedding scheme reproduces the main features of the fully wavefunction-based description.

With the results of the calculations including the ligands, we can summarize the general aspects of modeling the actinyl–ligand interaction: adding point charges on the equatorial plane introduces mixing of the $\Phi_{5/2u}$ and $\Delta_{3/2u}$ states, but underestimates the relative destabilization of the f^{ϕ} orbitals relative to the f^{δ} or f^{π} ones. Placing spherical finite volume Cl^- ions in place of the point charges does not change this picture. Allowing the charge density of the ligands to polarize gives the correct picture with the FDE freeze-and-thaw description underestimating slightly the relative destabilization of the f^{ϕ} orbitals. This is probably due to incomplete description of the orbital interactions between the chloride ligands and the metal orbitals in the density-only embedding description.

The inclusion of the rest of the crystal environment as an embedding potential to the calculation on $\text{NpO}_2\text{Cl}_4^{2-}$, brings only modest changes to the excitation energies, usually by no more than $100\text{--}200\text{ cm}^{-1}$ for the states with Δ and Φ character, a strong evidence that the bulk of the environment effects come from the equatorial ligands rather than from electrostatic interaction with the structural units further away. It is interesting to note that the environment seems to stabilize the states with dominant Φ character and destabilize states with dominant Δ character. This may be the effect of the 12 Cs^+ ions adjacent to the central unit that will polarize the equatorial ligands, thereby drawing charge away from the f^{ϕ} orbitals. The Π states experience differential environmental effects (about 800 cm^{-1} for **IV** but about 4000 cm^{-1} for **V**).

We conclude this section by noting that the calculated vertical excitation energies in this proof-of-principle application should of course not be blindly compared to the adiabatic excitation energies that are measured in experiment. The deviation between the two will be largest for states that are structurally different from the ground-state, in particular the Π states, where the excitation moves the electron from a non-bonding to a partially antibonding orbital. In these cases (states **IV** and **V**) the adiabatic excitation energies are likely to be significantly lower. In comparison to the results of Matsika and Pitzer, who did consider adiabatic effects in their calculations, our embedded cluster calculations are able to better approach the experimental results for the lowest excited states (**I** and **II**) but agree less well from **III** onwards as should be expected. Finally, another possible source of errors relative to the experimental data comes from the coupled cluster

treatment for which the active space was chosen to be somewhat smaller than previously used in our benchmark gas phase calculations. The latter calculations indicate that the effect of increasing electron correlation in the calculations, could also improve the agreement between the WFT-in-DFT embedding calculations and the experimental results as correlation appears to decrease the excitation energies for most states.

V. Conclusions

We have presented here a simple scheme to incorporate the effect of a frozen environment treated using DFT in the wavefunction-based calculation of excitation energies. In contrast to previously described WFT-in-DFT schemes,^{50,52} we do not use the electron density of the active subsystem to update the embedding potential. Instead, we assume that the ground state density obtained with DFT is identical to the density that will arise from a correlated *ab initio* treatment. In cases where TDDFT cannot be applied, such as charge-transfer excitations or open-shell systems with close-lying excited states, this assumption is often justified.

We have applied this WFT-in-DFT embedding scheme in two proof-of-concept applications, the calculation of the solvatochromic shift of acetone in water and the spectrum of NpO_2^{2+} embedded in a $\text{Cs}_2\text{UO}_2\text{Cl}_4$ crystal. For acetone in water, we show that the embedding potential is able to correctly describe the effect of the environment on the $n \rightarrow \pi$ excitation energies both in TDDFT and in CC2 calculations. The efficiency of the WFT-in-DFT embedding scheme makes it possible to perform CC2 calculations for acetone surrounded by a solvent shell of water for 220 different snapshots obtained from an MD simulation, thus making it possible to accurately include the effects of the dynamics on the solvatochromic shift.

For NpO_2^{2+} embedded in a $\text{Cs}_2\text{UO}_2\text{Cl}_4$ crystal, we find that our WFT-in-DFT embedding scheme is able to incorporate the effect of the crystal environment in IHFSCC calculations of the electronically excited states. In particular, the embedding scheme is able to closely reproduce the spectrum of $\text{NpO}_2\text{Cl}_4^{2-}$ calculated within a fully wavefunction-based treatment, provided we allow the density of the chloride ligands to be polarized. While such an agreement depends on the localized nature of the transitions under consideration, it introduces an economical yet highly accurate way to compute the $f\text{--}f$ spectra of actinyl ions in complex environments because they can be treated in a 3-atom wave function model.

In both applications, which consider two very different environments, we see that the WFT-in-DFT FDE method is capable of accurately representing the environment. The remaining discrepancies mainly originate from intrinsic errors in the description of the subsystems (such as incomplete basis sets, the degree of electron correlation recovered by the wavefunction-based methods) while deficiencies of the embedding procedure itself are small. This indicates that our initial assumption that the ground-state density of the embedded system is described accurately by DFT is indeed valid for the investigated systems. This makes the WFT-in-DFT approach an interesting and cost-effective solution for applications where DFT is known to yield accurate densities but TDDFT

fails (such as charge-transfer excitations or open-shell systems).

Further work is necessary in situations where DFT is not able to accurately describe the ground state density of the active part, or in cases in which the excitation studied does significantly change the density overlap between the embedded system and its surrounding environment. We are currently working on a generalization of the implementation that allows proper treatment of such cases as well.

Note added in proof

Very recently, an inconsistency in the ADF implementation of the PW91k functional for the spin-restricted case was reported in ref. 109. Although the effect on our results turned out to be insignificant, all data in this paper were corrected accordingly.

Acknowledgements

The authors thank The Netherlands Organization for Scientific Research (NWO) for financial support *via* the TOP and the Vici programs and acknowledge computer time provided by the Dutch National Computing Facilities (NCF). We would further like to express our gratitude to Dr Manuel Louwse (VU Amsterdam) and Dr Johannes Neugebauer (ETH Zurich) for kindly providing us with the geometric data for acetone in the gas-phase and solution, as well as to Dr Florent Réal (PhLAM, Université de Lille 1/CNRS) for generating the embedded cluster coordinates and the Made- lung potential for Cs₂UO₂Cl₄.

References

- 1 F. Furche and D. Rappoport, in *Computational Photochemistry*, ed. M. Olivucci, Computational and Theoretical Chemistry, Elsevier, Amsterdam, 2005, ch. 3, vol. 16.
- 2 A. Dreuw and M. Head-Gordon, *Chem. Rev.*, 2005, **105**, 4009–4037.
- 3 B. Ordejón, M. Karbowiak, L. Seijo and Z. Barandiarán, *J. Chem. Phys.*, 2006, **125**, 074511.
- 4 M. E. Casida, in *Recent Advances in Density-Functional Methods*, ed. D. P. Chong, World Scientific, Singapore, 1995, pp. 155–192.
- 5 R. van Leeuwen, *Int. J. Mod. Phys. B*, 2001, **15**, 1969.
- 6 C. Hättig and A. Köhn, *J. Chem. Phys.*, 2002, **117**, 6939–6951.
- 7 D. Kats, T. Korona and M. Schütz, *J. Chem. Phys.*, 2006, **125**, 104106.
- 8 D. Kats, T. Korona and M. Schütz, *J. Chem. Phys.*, 2007, **127**, 064107.
- 9 A. Warshel and M. Levitt, *J. Mol. Biol.*, 1976, **103**, 227–249.
- 10 P. Sherwood, in *Modern Methods and Algorithms of Quantum Chemistry*, ed. J. Grotendorst, NIC Series, John von Neumann Institute for Computing, Jülich, 2000, vol. 1, pp. 257–277.
- 11 J. Gao, in *Reviews in Computational Chemistry*, ed. K. B. Lipkowitz and D. B. Boyd, VCH, New York, 1995, vol. 7, pp. 119–185.
- 12 A. Warshel and Z. T. Chu, *J. Phys. Chem. B*, 2001, **105**, 9857–9871.
- 13 R. Rajamani and J. Gao, *J. Comput. Chem.*, 2001, **23**, 96–105.
- 14 M. A. L. Marques, X. López, D. Varsano, A. Castro and A. Rubio, *Phys. Rev. Lett.*, 2003, **90**, 258101.
- 15 A. Sergi, M. Grüning, M. Ferrario and F. Buda, *J. Phys. Chem. B*, 2001, **105**, 4386–4391.
- 16 U. F. Röhrig, I. Frank, J. Hutter, A. Laio, J. VandeVondele and U. Rothlisberger, *ChemPhysChem*, 2003, **4**, 1177–1182.
- 17 S. Humbel, S. Sieber and K. Morokuma, *J. Chem. Phys.*, 1996, **105**, 1959–1967.
- 18 M. Svensson, S. Humbel, R. Froese, T. Matsubara, S. Sieber and K. Morokuma, *J. Phys. Chem.*, 1996, **100**, 19357–19363.
- 19 L. Seijo and Z. Barandiarán, *J. Chem. Phys.*, 2004, **121**, 6698–6709.
- 20 L. Seijo, Z. Barandiarán and J. M. Soler, *Theor. Chem. Acc.*, 2007, **118**, 541–547.
- 21 Z. Barandiarán and L. Seijo, *J. Chem. Phys.*, 1988, **89**, 5739–5746.
- 22 L. Seijo, Z. Barandiarán and E. Harguindey, *J. Chem. Phys.*, 2001, **114**, 118–129.
- 23 B. Ordejón, L. Seijo and Z. Barandiarán, *J. Chem. Phys.*, 2005, **123**, 204502.
- 24 B. Swerts, C. L. F. Chibotaru, R. Lindh, L. Seijo, Z. Barandiarán, S. Clima, K. Pierloot and F. A. Hendrickx, *J. Chem. Theory Comput.*, 2008, **4**(4), 586–594.
- 25 T. A. Wesolowski and A. Warshel, *J. Phys. Chem.*, 1993, **97**, 8050–8053.
- 26 J. Neugebauer, M. J. Louwse, E. J. Baerends and T. A. Wesolowski, *J. Chem. Phys.*, 2005, **122**, 094115.
- 27 J. Neugebauer, Ch. R. Jacob, T. A. Wesolowski and E. J. Baerends, *J. Phys. Chem. A*, 2005, **109**, 7805–7814.
- 28 Ch. R. Jacob, J. Neugebauer, L. Jensen and L. Visscher, *Phys. Chem. Chem. Phys.*, 2006, **8**, 2349–2359.
- 29 J. Neugebauer and E. J. Baerends, *J. Phys. Chem. A*, 2006, **110**, 8786–8796.
- 30 J. M. García-Lastra, T. Wesolowski, M. T. Barriuso, J. A. Aramburu and M. Moreno, *J. Phys.: Condens. Matter*, 2006, **18**, 1519–1534.
- 31 M. Zbiri, C. A. Daul and T. A. Wesolowski, *J. Chem. Theory Comput.*, 2006, **2**(4), 1106–1111.
- 32 J. Neugebauer, *J. Chem. Phys.*, 2007, **126**, 134116.
- 33 J. Neugebauer, *J. Phys. Chem. B*, 2008, **112**, 2207–2217.
- 34 D. J. Tozer, *J. Chem. Phys.*, 2003, **119**, 12697–12699.
- 35 M. E. Casida, F. Gutierrez, J. Guan, F.-X. Gadea, D. Salahub and J.-P. Daudey, *J. Chem. Phys.*, 2000, **113**, 7062–7071.
- 36 A. Dreuw, J. L. Weisman and M. Head-Gordon, *J. Chem. Phys.*, 2003, **119**, 2943–2946.
- 37 J. Neugebauer, O. Gritsenko and E. J. Baerends, *J. Chem. Phys.*, 2006, **124**, 214102.
- 38 O. Gritsenko and E. J. Baerends, *J. Chem. Phys.*, 2004, **121**, 655–660.
- 39 M. Wanko, M. Hoffmann, P. Strodel, A. Koslowski, W. Thiel, F. Neese, T. Frauenheim and M. Elstner, *J. Chem. Phys. B*, 2005, **109**, 3606–3615.
- 40 A. Dreuw, *ChemPhysChem*, 2006, **7**, 2259–2274.
- 41 D. Rappoport and F. Furche, *J. Am. Chem. Soc.*, 2004, **126**, 1277–1284.
- 42 A. Köhn and C. Hättig, *J. Am. Chem. Soc.*, 2004, **126**, 7399–7410.
- 43 C. Hättig, A. Hellweg and A. Köhn, *J. Am. Chem. Soc.*, 2006, **128**, 15672–15682.
- 44 M. E. Casida, *J. Chem. Phys.*, 2005, **122**, 054111.
- 45 N. T. Maitra, F. Zhang, R. J. Cave and K. Burke, *J. Chem. Phys.*, 2004, **120**, 5932–5937.
- 46 S. A. Cotton, *Annu. Rep. Prog. Chem., Sect. A*, 2006, **102**, 308.
- 47 M. D. Ward, *Annu. Rep. Prog. Chem., Sect. A*, 2006, **102**, 584.
- 48 N. Govind, Y. A. Wang, A. J. R. da Silva and E. A. Carter, *Chem. Phys. Lett.*, 1998, **295**, 129–134.
- 49 N. Govind, Y. A. Wang and E. A. Carter, *J. Chem. Phys.*, 1999, **110**, 7677–7688.
- 50 P. Huang and E. A. Carter, *J. Chem. Phys.*, 2006, **125**, 084102.
- 51 T. Klüner, N. Govind, Y. A. Wang and E. A. Carter, *Phys. Rev. Lett.*, 2001, **86**, 5954–5957.
- 52 T. Klüner, N. Govind, Y. A. Wang and E. A. Carter, *J. Chem. Phys.*, 2002, **116**, 42–54.
- 53 I. Infante, A. S. P. Gomes and L. Visscher, *J. Chem. Phys.*, 2006, **125**, 074301.
- 54 T. A. Wesolowski, *Phys. Rev. Lett.*, 2002, **88**, 209701.
- 55 T. Klüner, N. Govind, Y. A. Wang and E. A. Carter, *Phys. Rev. Lett.*, 2002, **88**, 209702.
- 56 T. A. Wesolowski, *Phys. Rev. A*, 2008, **77**, 012504.
- 57 T. A. Wesolowski, *J. Chem. Phys.*, 1997, **106**, 8516–8526.
- 58 T. A. Wesolowski, P.-Y. Morgantini and J. Weber, *J. Chem. Phys.*, 2002, **116**, 6411–6421.
- 59 R. Kevorkyants, M. Dulak and T. A. Wesolowski, *J. Chem. Phys.*, 2006, **124**, 024104.

- 60 J. Neugebauer, M. J. Louwerse, P. Belanzoni, T. A. Wesolowski and E. J. Baerends, *J. Chem. Phys.*, 2005, **123**, 114101.
- 61 R. E. Bulo, Ch. R. Jacob and L. Visscher, *J. Phys. Chem. A*, 2008, **112**, 2640–2647.
- 62 P. Cortona, *Phys. Rev. B*, 1992, **46**, 2008–2014.
- 63 P. Cortona, A. Villaflorita Monteleone and P. Becker, *Int. J. Quantum Chem.*, 1995, **56**, 831–837.
- 64 P. Cortona and A. Villaflorita Monteleone, *J. Phys.: Condens. Matter*, 1996, **8**, 8983–8994.
- 65 W. N. Mei, L. L. Boyer, M. J. Mehl, M. M. Ossowski and H. T. Stokes, *Phys. Rev. B*, 2000, **61**, 11425–11431.
- 66 M. M. Ossowski, L. L. Boyer, M. J. Mehl and H. T. Stokes, *Phys. Rev. B*, 2002, **66**, 224302.
- 67 Ch. R. Jacob and L. Visscher, *J. Chem. Phys.*, 2008, **128**, 155102.
- 68 T. A. Wesolowski and J. Weber, *Chem. Phys. Lett.*, 1996, **248**, 71–76.
- 69 M. Dulak and T. A. Wesolowski, *J. Chem. Theory Comput.*, 2006, **2**, 1538–1543.
- 70 M. E. Casida and T. A. Wesolowski, *Int. J. Quantum Chem.*, 2004, **96**, 577–588.
- 71 ADP, Amsterdam density functional program (development version), Theoretical Chemistry, Vrije Universiteit Amsterdam, URL: <http://www.scm.com>, 2008.
- 72 G. te Velde, F. M. Bickelhaupt, E. J. Baerends, C. Fonseca Guerra, S. J. A. van Gisbergen, J. G. Snijders and T. Ziegler, *J. Comput. Chem.*, 2001, **22**, 931–967.
- 73 Ch. R. Jacob, J. Neugebauer and L. Visscher, *J. Comput. Chem.*, 2008, **29**, 1011–1018.
- 74 A. S. P. Gomes, F. Real, Ch. R. Jacob, V. Vallet and L. Visscher, 2008, in preparation.
- 75 S. H. Vosko, L. Wilk and M. Nusair, *Can. J. Phys.*, 1980, **58**, 1200–1211.
- 76 E. van Lenthe and E. J. Baerends, *J. Comput. Chem.*, 2003, **24**, 1142–1156.
- 77 P. R. T. Schipper, O. V. Gritsenko, S. J. A. van Gisbergen and E. J. Baerends, *J. Chem. Phys.*, 2000, **112**, 1344–1352.
- 78 E. van Lenthe, J. G. Snijders and E. J. Baerends, *J. Chem. Phys.*, 1996, **105**, 6505–6516.
- 79 A. Lembarki and H. Chermette, *Phys. Rev. A*, 1994, **50**, 5328–5331.
- 80 A. D. Becke, *Phys. Rev. A*, 1988, **38**, 3098–3100.
- 81 J. P. Perdew, J. A. Chevary, S. H. Vosko, K. A. Jackson, M. R. Pederson, D. J. Singh and C. Fiolhais, *Phys. Rev. B*, 1992, **46**, 6671–6687.
- 82 DALTON, a molecular electronic structure program, Release 2.0 (2005), see <http://www.kjemi.uio.no/software/dalton/dalton.html>, 2005.
- 83 DIRAC, a relativistic *ab initio* electronic structure program, Release DIRAC04.0 written by H. J. Aa. Jensen, T. Saue, L. Visscher with contributions from V. Bakken, E. Eliav, T. Enevoldsen, T. Fleig, O. Fossgaard, T. Helgaker, J. Laerdahl, C. V. Larsen, P. Norman, J. Olsen, M. Pernpointner, J. K. Pedersen, K. Ruud, P. Salek, J. N. P. van Stralen, J. Thyssen, O. Visser and T. Winther, URL: <http://dirac.chem.sdu.dk>, 2004.
- 84 G. te Velde and E. J. Baerends, *J. Comput. Phys.*, 1992, **99**, 84–98.
- 85 H. Koch, P. Jorgensen and J. Olsen, *Chem. Phys. Lett.*, 1995, **244**, 75–82.
- 86 O. Christiansen, H. Koch, P. Halkier, Asger Jorgensen, T. Helgaker and A. S. de Méras, *J. Chem. Phys.*, 1996, **105**, 6921.
- 87 K. Hald, C. Hättig and P. Jorgensen, *J. Chem. Phys.*, 2000, **113**, 7765.
- 88 T. H. Dunning, *J. Chem. Phys.*, 1989, **90**, 1007–1023.
- 89 K. Aidas, J. Kongsted, A. Osted, K. Mikkelsen and O. Christiansen, *J. Phys. Chem. A*, 2005, **109**, 8001–8010.
- 90 M. Iliaš and T. Saue, *J. Chem. Phys.*, 2007, **126**, 064102.
- 91 Program AMFI, B. Schimmelpennig, Stockholm University, Sweden.
- 92 B. A. Hess, C. M. Marian, U. Wahlgren and O. Gropen, *Chem. Phys. Lett.*, 1996, **251**, 365–371.
- 93 K. G. Dyall, *Theor. Chem. Acc.*, 2006, **90**, 491–500.
- 94 A. Landau, E. Eliav, Y. Ishikawa and U. Kaldor, *J. Chem. Phys.*, 2000, **113**, 9905–9910.
- 95 A. Landau, E. Eliav, Y. Ishikawa and U. Kaldor, *J. Chem. Phys.*, 2001, **115**, 6862–6865.
- 96 L. Visscher, E. Eliav and U. Kaldor, *J. Chem. Phys.*, 2001, **115**(21), 9720–9726.
- 97 Ch. R. Jacob, R. E. Bulo and L. Visscher, 2008, in preparation.
- 98 R. G. Denning, J. O. W. Norris and D. Brown, *Mol. Phys.*, 1982, **46**, 287–323.
- 99 R. G. Denning, J. O. W. Norris and D. Brown, *Mol. Phys.*, 1982, **46**, 325–364.
- 100 S. Matsika and R. M. Pitzer, *J. Phys. Chem. A*, 2001, **105**, 637–645.
- 101 D. J. Watkin, R. G. Denning and K. Prout, *Acta Crystallogr., Sect. C*, 1991, **47**, 2517–2519.
- 102 F. Real, 2007, private communication.
- 103 A. Gelle and M.-B. Lepetit, *J. Chem. Phys.*, 2008, in press.
- 104 A. Gelle and M.-B. Lepetit, Fast calculation of the electrostatic potential in ionic crystals by direct summation method, arXiv:cond-mat.str-el/0711.2888, 2007.
- 105 M. P. Wilkerson, C. A. Arrington, J. M. Berg and B. L. Scott, *J. Alloys Compd.*, 2007, **444**, 634–639.
- 106 C. W. Porter and C. Iddings, *J. Am. Chem. Soc.*, 1926, **48**, 40–44.
- 107 N. S. Bayliss and E. G. McRae, *J. Phys. Chem.*, 1954, **58**, 1006–1011.
- 108 N. S. Bayliss and G. Wills-Johnson, *Spectrochim. Acta, Part A*, 1968, **24**, 551.
- 109 S. Fux, K. Kiewisch, Ch. R. Jacob, J. Neugebauer and M. Reiher, *Chem. Phys. Lett.*, submitted.